










Research Article

Iron Oxide Nanoparticles: Preparation, Characterization, and Assessment of Antimicrobial and Anticancer Activity

Abdulaziz Alangari ¹, Mohammed S. Alqahtani ², Ayesha Mateen ¹,
Mohd Abul Kalam ², Abdullah Alshememry ², Raisuddin Ali ², Mohsin Kazi ²,
Khalid M. AlGhamdi ³ and Rabbani Syed ²

¹Department of Clinical Laboratory Sciences, College of Applied Medical Sciences, King Saud University, P.O. Box 10219, Riyadh 11433, Saudi Arabia

²Department of Pharmaceutics, College of Pharmacy, P.O. Box 2457, King Saud University, Riyadh, 11451, Saudi Arabia

³Department of Dermatology, College of Medicine, King Saud University, Riyadh, 11451, Saudi Arabia

Correspondence should be addressed to Rabbani Syed; rsyed@ksu.edu.sa

Received 26 December 2021; Revised 21 January 2022; Accepted 1 February 2022; Published 11 March 2022

Academic Editor: Lakshmipathy R

Copyright © 2022 Abdulaziz Alangari et al. This is an open access article distributed under the Creative Commons Attribution License, which permits unrestricted use, distribution, and reproduction in any medium, provided the original work is properly cited.

Nanotechnology and nanoparticles (NPs) have increasingly been studied as an alternative for antibiotics because of the feasibility to be used in implantable devices both for bacterial detection and infection prevention. The low rate of resistance development against NPs because of its multiple mode of action has contributed to its increased acceptance in clinical setting. Further development of NPs and their anticancer activity against many human cancer cell lines including breast and ovarian have been documented. Fe₂O₃-NPs could be used for antibacterial and anticancer activity assessment. Iron oxide, apart from being available extensively and cheap, also plays a role in multiple biological processes, making it an interesting metal for NPs. The aim of the present study revolves around generation and characterization of iron oxide Fe₂O₃-NPs, followed by assessment of its antimicrobial and anticancer activities. Synthesis of Fe₂O₃-NPs was performed by hydrothermal approach, and its characterization was done by UV-visible, X-ray diffraction (XRD), Fourier-transform infrared spectroscopy (FTIR) analyses, and transmission electron microscopy (TEM). Antimicrobial activity was checked by agar diffusion assay against *Bacillus subtilis*, *Pseudomonas aeruginosa*, *Staphylococcus aureus*, *Escherichia coli*, and *Candida albicans*. Anticancer activity of the NPs was assessed using the human cancer cell lines including cervical carcinoma cell line (HeLa) and MCF7. The developed Fe₂O₃-NPs exhibited a characteristic absorption curve in the 500-600 nm wavelength range by UV-visible analysis, the XRD peaks were found to index the rhombohedral shape, and the FTIR analysis ascertained the bonds and functional groups at wavenumber from 400 to 4000 cm⁻¹. Antimicrobial assay detected significant effect against *Staphylococcus aureus* and *Bacillus subtilis* with zones of inhibition: 21 and 22 mm, respectively. Likewise, Fe₂O₃-NPs show good activity towards tested fungal strain *Candida albicans* with zone of inhibition of 24 mm. The 2,5-diphenyl-2H-tetrazolium bromide (MTT) assay identified significant anticancer activity of the NPs against both cell lines. Our study documents the successful generation and characterization of Fe₂O₃-NPs having excellent antimicrobial and anticancer activities.

1. Introduction

Nanotechnology, as a technology-fueled science, has recently gained enormous attention because of the ability to engineer functional systems including drug delivery systems and diagnostic fundamentals in molecular size, which also form the pillars of nanomedicine that has designed many success-

ful drug delivery systems to mankind [1]. Nanotechnology has been successfully implemented to design novel drug delivery systems using nanoparticles (NPs) which have today also contributed to precision medicine. Advances in nanoparticle designs have ensured the NPs can overcome the heterogenous delivery barriers and can intelligently improve efficacy [2]. NPs are classified based on their shape,

size, and properties, the major groups include metal, ceramic, polymeric, and fullerenes, and the sizes range between 1 and 100 nm [3]. Further, NPs are structurally complex and consist of three layers including the functional surface layer with metal ions, surfactants, or polymers, the shell layer, and the core that refers to the NP [4]. NPs are sized similar to the macromolecules inside the human body and take advantage of the existing cellular machinery to facilitate its intent-of-action. NPs have also successfully aided in reducing drug toxicity and side effects due to high efficacy delivery that ensures therapeutic potential in minimal dosage, supports sustained drug release, and alters drug distribution, as well as clearance [5]. The National Nanotechnology Initiative (NNI) in the year 2000 by the US National Science and Technology Council (NSTC) facilitated the realization and translation of nanotechnology in clinical settings, and since then, multiple studies have recorded the significance of NPs in respiratory diseases, kidney diseases, and antibacterial and anticancer agents [6–8]. Although research has documented significant strides in application of NPs, the translation at patient levels is low majorly due to patient heterogeneity, as well as difference in physiology between animals and humans [9].

The discovery of antibiotics in the 20th century with Salvarsan for syphilis has been documented to be significant for mankind, and the accidental discovery of penicillin fueled antibiotic research marked as the golden age [10–12]. However, in the current scenario, with increase in number of antibiotic resistances, the number of agencies involved in research for new antibiotics has gone down and to address this deficit, the World Health Organization (WHO) published the Global Priority Pathogens List (PPL) in the year 2017 [13]. The metal-NPs have been popularly studied as a solution to tackle antibiotic resistance because of their ability to target multiple biomolecular aspects among resistant strains. The main mechanisms of killing have been attributed to cation release, production of reactive oxygen species (ROS), ATP depletion, and membrane interaction to cite a few. It has also been postulated that emergence of antibacterial NPs has the potential to curb evolution of more resistant strains. The metals popularly used to fabricate antibacterial NPs include aluminum (Al_2O_3), iron (Fe_2O_3), magnesium (MgO), zinc (ZnO), bismuth, and cerium. [14]. Studies have demonstrated the use of metallic NPs to improve antimicrobial efficiency against morphologically distinct pathogens in healthcare, and one such demonstrated the impact of tungsten carbide, silver, and copper NPs against two hospital acquired pathogens: *Staphylococcus aureus* and *Pseudomonas aeruginosa* [15].

Cancer is a multifaceted and clinically challenging disease due to variable disease presentation, progression, and recurrence. Though precision medicine is popular in cancer treatment and management involving study of the genetic signature to classify somatic and germline variations, the feasibility to ensure the anticancer agent is able to deliver targeted impact is still lacking causing unwarranted injury to the patient [16]. The unique characteristics of NPs including large surface-to-volume ratio, ease of synthesis, and broad optical properties allow development of new and effi-

cient therapeutic strategies for cancer. Studies have assessed the anticancer impact of silver NPs (AgNPs) on different cancer cell lines with respect to decrease in cell motility and viability, promotion of ROS, and impairment of MMP-2 and MMP-9 activity culminating in autophagy- and apoptosis-induced cell death [17]. Another study evaluated the impact of gold, iron oxide, and ZnO NPs on colorectal cancer cell HT29 found the iron oxide NPs to exhibit a cytotoxicity of 26.98% at concentration of 50 $\mu\text{g}/\text{ml}$, while zinc oxide NPs were found to exhibit significant anticancer activity [18]. This study proves that the inorganic component of the NPs has directed action only against certain cancer types. The iron oxide NPs have demonstrated safety, considerable clinical utility, and the FDA-approved applications include cancer diagnosis and for hyperthermia treatment [19].

The aim of our study revolves around synthesis and characterization of iron oxide Fe_2O_3 -NPs followed by its antibacterial and anticancer activity assessment. Iron oxide, apart from being available extensively and cheap, also plays a role in multiple biological processes, making it an interesting metal for NPs. The three common forms of iron oxide in nature include the magnetite (Fe_3O_4), maghemite ($\gamma\text{-Fe}_2\text{O}_3$), and hematite ($\alpha\text{-Fe}_2\text{O}_3$) [20]. We believe the emerging field of nanomedicine will greatly benefit with increasing information around assessment of NP potential to aid the development of nontoxic chemotherapy as well as minimize development of multidrug resistant bacterial strains.

2. Materials and Methods

There are many methods for synthesis of metal and metal oxide NPs including the physical method top-down approach, the thermolysis method, chemical reduction, biochemical, electrochemical, wave-assisted, cementation, and biological methods each having its own set of proven application [21]. The synthesis of Fe_2O_3 -NPs was done using analytical grade chemical cast-offs without further purification. The Iron (III) Chloride Hexahydrate ($\text{FeCl}_3 \cdot 6\text{H}_2\text{O}$) (purity $\geq 98\%$) and ammonia hydroxide (NH_4OH) for synthesis were procured from Sigma-Aldrich, St. Louis, MO, USA, while the deionized water was obtained from Milli-Q[®] ultrapure water purification system (Nihon Millipore Ltd., Tokyo, Japan).

2.1. Synthesis of Fe_2O_3 -NPs. The synthesis of Fe_2O_3 -NPs was done by the hydrothermal approach. The process involved dissolution of 0.85 mg of $\text{FeCl}_3 \cdot 6\text{H}_2\text{O}$ in 100 mL of double distilled water in a 250 mL round bottom flask followed by magnetic stirring (at 800 rpm) for 45 min at 85°C. An addition of 50 mL of NH_4OH was done to maintain the pH value of 11. The reaction mixture was then heated hydrothermally in a stainless steel Teflon lined Parr Autoclave at $160 \pm 5^\circ\text{C}$ for 12 h. Initially, the Ferric-Chloride Hexahydrate was yellow colored solid, and as the completion of reaction took place, it turned reddish brown similar to rust color. The color change was considered as the endpoint of the reaction and considered as an indicative of formation of Fe_2O_3 -NP. The resulting precipitate was separated by centrifugation at

8000 rpm and washed with double distilled water and ethanol for five times followed by drying in oven at 80°C. The product obtained was further calcined at 700°C for 4 h.

2.2. Particle Size, Polydispersity Index, and Zeta Potential Measurement. The hydrodynamic diameter (particle size), polydispersity index, and zeta potential of the developed Fe₂O₃-NPs were obtained through Zetasizer Nano-Series (Nano-ZS90, Malvern Instruments, England) at 25°C at the scattering angle of 90° for the optimum possible detection [22]. The zeta potential of the NPs was also determined by the same instrument using software DTS-Version 4.1 (Malvern, England). Prior to DLS measurements, the NPs were properly suspended and diluted with Milli-Q water. All the measurements were performed in triplicate.

2.3. Characterization of the Fe₂O₃-NPs. Initial surface characterization was done using UV-visible analysis of the as-synthesized Fe₂O₃ NP using the Lambda-35 Instrument (Perkin Elmer, Waltham, MA, USA). The UV-Vis spectrophotometry analysis at different time intervals of the reaction provides key information on the success of generation of the NPs. Further, bond level characterization by Fourier-transform infrared (FTIR) spectroscopy of the Fe₂O₃-NPs was recorded on a 1000 FTIR instrument (Perkin-Elmer, Waltham, MA, USA). The formation and crystallinity of the prepared Fe₂O₃-NPs were also confirmed by using the powder diffraction technique (Ultima IV, X-ray Diffractometer, Rigaku, Inc. Japan). The size and shape of the as-synthesized Fe₂O₃-NPs were investigated using transmission electron microscopy (TEM) (Jeol TEM model JEM-1101 (Japan)). The TEM analysis provides insight on the morphology of the biosynthesized NPs.

2.4. Assessment of Antimicrobial Activity. The antimicrobial activity of the synthesized Fe₂O₃-NP was done by the agar diffusion technique. The bacterial strains used for the assessment were procured from the Department of Pharmaceutics, Microbiology, College of Pharmacy, King Saud University. The microbial strains were selected from the Global Priority Pathogens List which is one of the major objective for the assessment of antimicrobial activity. Total five American type culture collection (ATCC) pure cultures of *Escherichia coli* (*E. coli*), *Bacillus subtilis* (*B. subtilis*), *Pseudomonas aeruginosa* (*P. aeruginosa*), *Staphylococcus aureus* (*S. aureus*), and *Candida albicans* (*C. albicans*) were tested for their antibiotic susceptibility profiles using the generated NPs. The agar diffusion method adopted was in accordance to a previous report [23]. The Mueller Hinton agar (MHA) plates were prepared for the testing purpose, and each of the strains was inoculated by the spread plate technique. This was followed by creating the wells of 6 mm diameter each using a sterile borer. In the first well, 30 µL of ampicillin (100 mg/mL) for bacterial strains and fluconazole for *Candida* (30 mg/mL) were added, in the next well, 100 µL of the prepared Fe₂O₃-NPs was inoculated, and in the last one, Mueller Hinton agar (MHA) media as positive control was added. The plates were further incubated at 37°C for

24 h in the incubator. The entire assessment was done in triplicates.

2.5. Assessment of Anticancer Activity. The anticancer activity of the synthesized Fe₂O₃-NPs was evaluated along with the median inhibitory dose (IC₅₀) on two different tumor cell lines, viz., the human cervical carcinoma cell line (HeLa) and MCF7 cell lines. Cytotoxicity assessment was done by harvesting each of the cell suspension at concentration of 5 × 10⁴ cell suspension in a 96-well flat bottom plate containing Dulbecco's modified Eagle medium (DMEM) with 5% fetal bovine serum. The prepared NPs were also seeded at different concentrations, viz., 100 µg/mL, 50 µg/mL, 25 µg/mL, 12.5 µg/mL, 6.2 µg/mL, and 3.1 µg/mL. The plate was then incubated at 37°C for 24 h in 5% CO₂ incubator. Post-incubation, the cells were washed with a serum-free medium containing 100 µL of 5 mg/mL 3-4,5 dimethylthiazol-2,5 diphenyl tetrazolium bromide (MTT) and further incubated for 4-5 h. Postincubation, the cells were further washed with phosphate buffer saline (PBS). Further, 100 µL of dimethyl sulfoxide (DMSO) was used to solubilize the unbound formazan, followed by reading of the plates at 570 nm absorbance using a plate reader (Biotek, USA). The entire assessment was done in triplicates, and the IC₅₀ was determined by the color intensity of the formazan dye which was equated to be directly proportional to the quantity of viable cells.

2.6. Statistical Analysis. T-test was used to compare the results of antimicrobial activity of the synthesized Fe₂O₃-NP and standard antimicrobials, where **p* < 0.05 is considered significant result.

3. Results

3.1. Particle Characterization. The hydrodynamic diameter and polydispersity index (PDI) of the developed Fe₂O₃-NPs were found to be 91.5 ± 4.5 nm and 0.251 ± 0.018, respectively, while the zeta potential was found to be 20.8 ± 2.26 mV. The size and zeta potential distributions of the Fe₂O₃-NPs are represented in Figure 1.

3.2. Characterization of Fe₂O₃-NPs

3.2.1. UV-Vis Analysis. The UV-Vis analysis confirmed the preparation of Fe₂O₃-NPs (Figure 2). The absorption spectra of Fe₂O₃-NPs dispersed in deionized water displayed a broad absorption peak at about 550 nm. The UV-Vis absorption spectra of Fe₂O₃-NPs displayed an absorption curve in the range of 500-600 nm wavelength and defines the characteristic of the synthesized NPs.

3.2.2. X-Ray Diffraction (XRD) Study. The X-ray diffraction (XRD) crystallography was used to assess structure and crystallinity of the synthesized Fe₂O₃-NPs (Figure 3). The XRD pattern of the α-Fe₂O₃-NPs prepared by hydrothermal approach was found to display the diffraction peak which was readily indexed to be rhombohedral (hexagonal), where α is known as lattice parameter. The wavelength of incident X-rays was set at 0.154 nm monochromatized with a graphite crystal. The space group of the rhombohedral structures

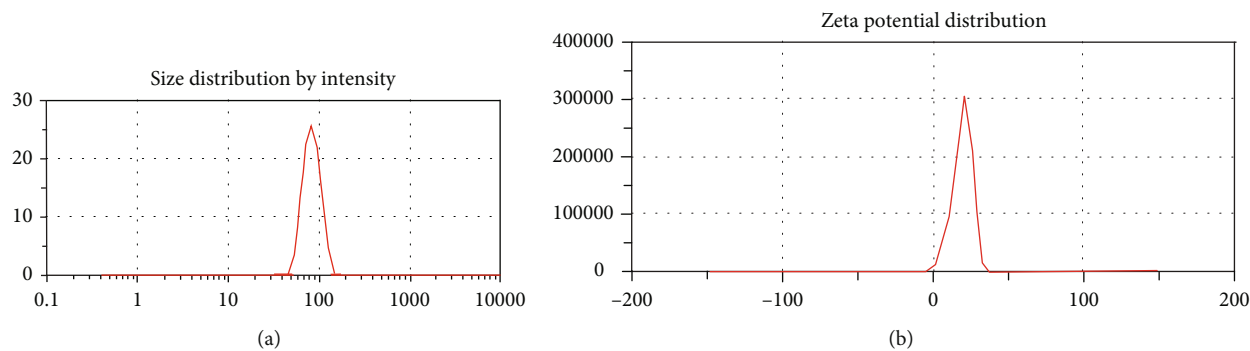


FIGURE 1: (a) Particle size and (b) zeta potential distributions of Fe_2O_3 -NPs.

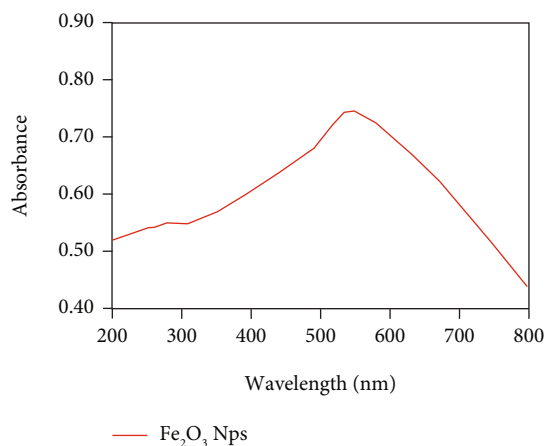


FIGURE 2: The UV-visible analysis of Fe_2O_3 -NPs.

was found to be $R\text{-}3c$, and the peaks detected at 2θ range of 24.15° (012), 33.10° (104), 35.53° (110), 40.59° (113), 49.49° (024), 54.11° (116) and 57.32° (018), 62.4° (214), 63.9° (300), 72.1° (1010), and 75.4° (220) confirm the crystalline structure corresponding to the $\alpha\text{-Fe}_2\text{O}_3$ -NPs [24]. These findings were in agreement with the previous studies [24, 25]. The standard values of the peak for magnetite and maghemite were found at 35.43° and 35.62° , respectively, as reported [26, 27]. In the present investigation, the diffraction angle for the developed Fe_2O_3 -NPs was 35.53° (110), which was more close to maghemite index than that of the magnetite index. This finding suggested the presence of predominantly maghemite lattice than that of magnetite (Fe_3O_4) lattice in the developed iron oxide NPs. Finally, the XRD peaks evidently represent the formation of the Fe_2O_3 -NPs.

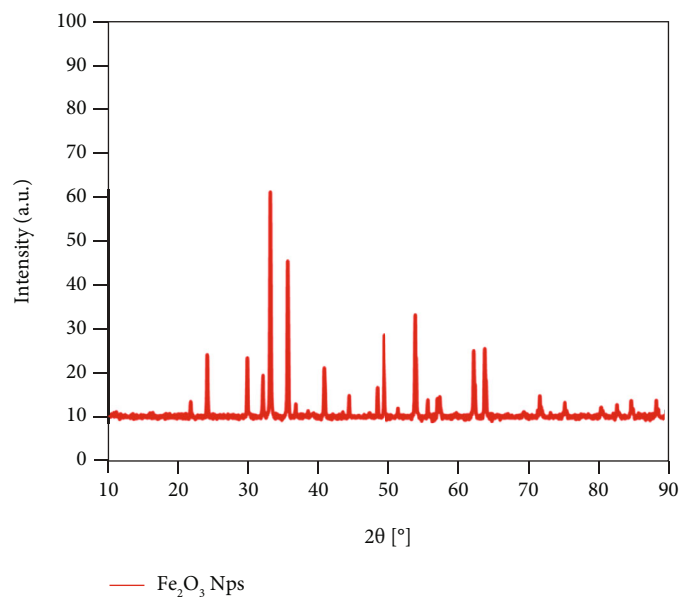
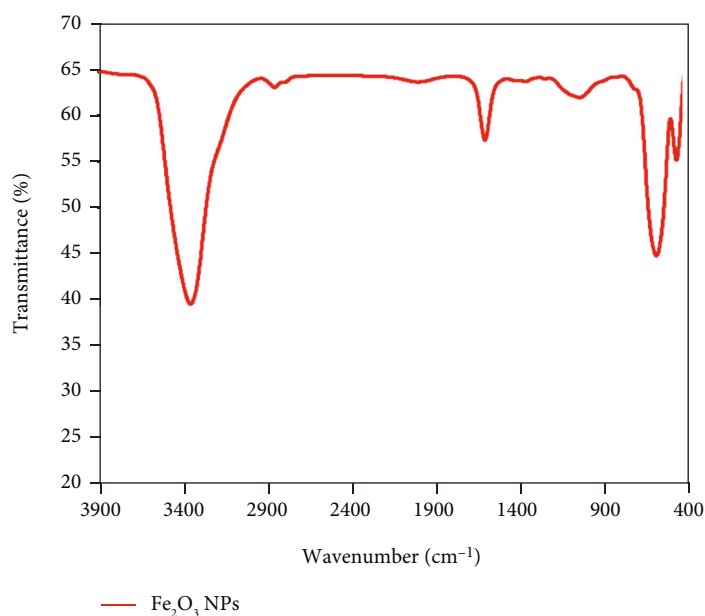
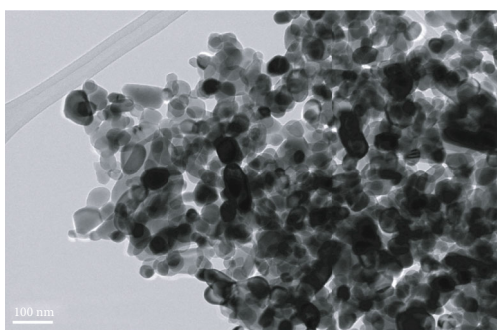
3.2.3. FTIR Analysis. The FTIR analysis of the synthesized Fe_2O_3 -NPs detected an outcome in the range of wavenumber $400\text{--}4000\text{ cm}^{-1}$ that ascertained the chemical bonds as well as functional groups (Figure 4). The FTIR spectrum of the synthesized Fe_2O_3 -NPs exhibited defined peaks at 517, 621, 1020, 1612, and 3435 cm^{-1} . The appearance of two well-defined peaks at 517 cm^{-1} and 621 cm^{-1} was due to the vibrational intrinsic stretching of metal oxygen bond vibrations (here, it was Fe-O), which indicated that the developed NPs were iron oxide [28, 29]. The presence of a

slightly dwarf peak at 1020 cm^{-1} was due to Fe-O asymmetric stretching. The absorption peaks appeared at 1612 cm^{-1} and 3431 cm^{-1} indicating the bending vibration of absorbed water and surface hydroxyl (-OH) groups, which might be due to the use of NH_4OH in the synthesis of the Fe_2O_3 -NPs [24]. These findings were further corroborated from the previous report which confirms that the developed NPs were iron oxide [28–31]. The FTIR analysis results thus were consistent with the confirmation accomplished from other additional executed characterization results.

3.3. Morphological Characterization of Fe_2O_3 -NPs by TEM Analysis. The morphological characterization of the developed Fe_2O_3 -NPs was performed by transmission electron microscopy. The TEM image (Figure 5) demonstrates the formation of spherical shape Fe_2O_3 -NPs, with an average size of $\sim 70\text{--}100\text{ nm}$. Mostly, the NPs were well dispersed, whereas some of these were slightly agglomerated. The few large particles were found which could be due to the agglomeration of smaller particles; however, the majority of the particles in the TEM images were less than 100 nm in size.

3.4. Antimicrobial Activity of the Synthesized Fe_2O_3 -NPs. The antimicrobial susceptibility was tested by agar diffusion method, and the results are summarized in Table 1. Compared to the standard ampicillin, Fe_2O_3 -NPs have shown significant antimicrobial activity against Gram positive bacteria *S. aureus* and *B. subtilis*, with zone of inhibition (ZOI): 21 mm and 22 mm , respectively ($p < 0.05$). However, Fe_2O_3 -NPs had no activity towards Gram negative strains *E. coli* and *P. aeruginosa*. Fe_2O_3 -NPs showed significant good susceptibility towards the tested fungal strain *C. albicans* in comparison to the standard fluconazole, and the zone of inhibition was 24 mm for Fe_2O_3 -NPs compared to 12 mm for fluconazole ($p < 0.05$).

3.5. Anticancer Activity of the Synthesized Fe_2O_3 -NPs. The synthesized Fe_2O_3 -NPs were further tested for anticancer activity against two cancer cell lines, namely, HepG2 and HeLa by the MTT assay. The generated Fe_2O_3 -NPs were found to significantly inhibit growth and proliferation of the MCF7 cells at IC_{50} of $53.35\text{ }\mu\text{g/mL}$. In case of HeLa cell line, the inhibition was found to be reasonable with IC_{50} of

FIGURE 3: The XRD patterns of the developed Fe₂O₃-NPs.FIGURE 4: FTIR spectrum of the developed Fe₂O₃-NPs.FIGURE 5: TEM image of Fe₂O₃-NPs.

68.12 $\mu\text{g/mL}$. The findings have been highlighted in Figures 6(a) and 6(b).

4. Discussion

This study documents the process of synthesis of Fe₂O₃-NPs followed by its structural classification as well as functional efficacy determination as an antimicrobial and anticancer activity. The drug absorption efficiency being inversely proportional to particle size makes NPs an exploitable drug delivery system, and studies have shown certain material coatings to increase accumulation and effect duration of

TABLE 1: Zone of inhibitions obtained during agar diffusion test by Fe_2O_3 -NPs as compared to ampicillin and fluconazole. Results were presented as mean \pm SD, $n = 3$.

Microorganisms	Zone of inhibitions (mm), mean \pm SD, $n = 3$		
	By ampicillin	By fluconazole	By Fe_2O_3 -NPs
<i>E. coli</i>	18.5 \pm 2.39	-	21.6 \pm 2.86
<i>B. subtilis</i>	14.8 \pm 1.75	-	22.5 \pm 2.55*
<i>P. aeruginosa</i>	19.5 \pm 2.75	-	19.8 \pm 1.98
<i>S. aureus</i>	13.5 \pm 1.83	-	21.4 \pm 2.35*
<i>C. albicans</i>	-	12.5 \pm 1.65	24.3 \pm 3.08*

* $p < 0.05$ (significant).

antimicrobial agent, for example, being increasing efficacy of daptomycin using chitosan-coated alginate NPs [32].

The Fe_2O_3 -NPs have gained popularity due to their unique properties including superparamagnetism (a form of magnetism appeared in very small-sized ferromagnetic or ferrimagnetic NPs), availability of greater surface area, and ease of separation along with the advantage of being inexpensive and role in many biological processes. Characteristic attributes of low toxicity and magnetism have made iron oxide NPs highly lucrative for biomedical applications involving drug delivery, thermal therapy, and magnetic resonance imaging (MRI) [33]. Our study involved generation of Fe_2O_3 -NPs by the hydrothermal approach followed by surface and structural characterization by UV-Vis, FTIR, XRD, TEM, particle size, and distribution. The UV-Vis analysis detected an absorbance peak at between 500 and 600 nm, a characteristic of iron oxide. Further, the XRD peaks indexed the synthesized NPs to rhombohedral structure with peaks appearing at 2θ range of 24.15° (012), 33.10° (104), 35.53° (110), 40.59° (113), 49.49° (024), 54.11° (116) and 57.32° (018), 62.4° (214), 63.9° (300), 72.1° (1010), and 75.4° (220). Studies have shown hematite minerals to have hexagonal structure [34]. The chemical bonds were ascertained by FTIR analysis, and the characteristic peak to Fe-O stretching mode of Fe_2O_3 -NPs was observed at 575 cm^{-1} . Similar studies on Fe_2O_3 -NPs have recorded observance of a broad peak at around 529.92 cm^{-1} by FTIR analysis, and the NPs were synthesized by a green protocol involving extract from *M. ornata* flower sheath extract [35]. Another recent study, which involved synthesis of green Fe_2O_3 -NPs from *Phoenix dactylifera*, was found to exhibit a sharp peak at 450 nm by UV-Vis spectrometry [36].

The particle size of the Fe_2O_3 -NPs was depending on the type of solvent used and chemical reaction time. Here, the size of the developed NPs was found in the nanorange (1-100 nm, for metallic nanoparticles). Slightly increased sizes were obtained during DLS technique ($\approx 91.5\text{ nm}$) because DLS measures the hydrodynamic diameter while TEM considers only the core sizes [37]. Although the average size of the NPs obtained using DLS was almost equal and in agreement with the observed sizes during TEM analysis. The low values of PDI (≈ 0.251) were obtained in DLS measurement confirming the narrow size distribution of the developed NPs. Generally, the Fe_2O_3 -NPs were found to have negative

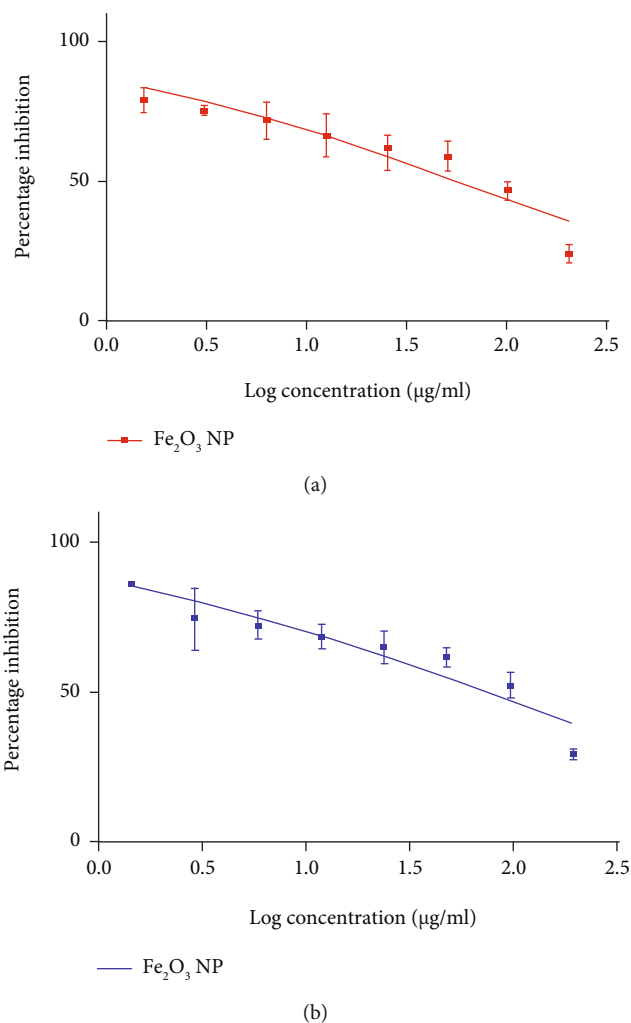


FIGURE 6: (a) Cell proliferation results of Fe_2O_3 -NPs in MCF7 cell lines. (b) Cell proliferation results of Fe_2O_3 -NPs in HeLa cell lines.

surface charges, where surface modification could provide high positively charged NPs for their better colloidal stabilization [26]. Contrary to this, in the present investigation, we obtained a sufficiently high positive charge ($\approx +20.8\text{ mV}$) on the surfaces of the developed Fe_2O_3 -NPs, which might be due to the use of NH_4OH in the synthesis of the NPs. The high surface positive charges could provide a stable dispersion to the Fe_2O_3 -NPs and prevent their unwanted aggregation, which was also suggested in the previous studies, where chitosan was used to obtain positively charged surface of the Fe_2O_3 -NPs [26, 38, 39].

When it comes to discussion around the antimicrobial properties of Fe_2O_3 -NPs, the mechanism of action is still under research and many studies have indicated conflicting reports with one indicating efficacy against *E. coli* which increased at increasing concentration, while some show no activity towards this pathogen [38, 40]. Studies have shown positive Fe_2O_3 -NPs to exhibit greater antimicrobial activity at lower concentrations than negative Fe_2O_3 -NPs. The string interaction has been documented to cause higher free energy change leading to increased production of the reactive oxygen species (ROS) [26]. Microscopic observation studies

have found magnetite (Fe_3O_4)-NPs to increase size of *Escherichia coli* (approximately 10-folds), and the bacterial cells were found to be clogged in between the magnetite-NPs because of its magnetic property. The antimicrobial activity of Fe_2O_3 -NPs synthesized by the *M. ornate* flower sheath has been tested activity against *S. aureus* and *S. agalactiae* [35]. A recent study has also reported that Fe_2O_3 -NPs exhibited antimicrobial activity against *S. dysenteriae* strain tested at different concentrations [41]. Devi et al. postulated that iron oxide nanoparticles (Fe-NPs) have efficient antifungal activity against various fungal strains [42]. Furthermore, Batool and co-authors have evaluated the antibacterial activity of Fe_2O_3 -NPs against multiple bacterial strains and identified maximum zone of inhibition against *E. coli* [36].

In the field of cancer research, the numerous clinical findings for the determination of multiple efficacy-affecting aspects of nanomedicine are crucial to combat the complexity around disease progression, treatment, management, and recurrence risk. In this case, balancing out efficacy versus impact on healthy cells is crucial to minimize impact to quality of life. There have been numerous studies which have discussed the success of Fe_2O_3 -NP injectable due to ensuing interaction between the NPs and the innate immune system. Further, the cancer therapy involving magnetic fluid hyperthermia is the treatment approved for humans involving use of Fe_2O_3 -NPs. Strategies including photothermal and photodynamic therapies involving Fe_2O_3 -NPs have demonstrated relevant potential in the preclinical settings [19]. Studies have documented Fe_2O_3 -NPs to bear the potential to activate the antitumor immune response, wherein exposure to starch-coated Fe_2O_3 -NPs triggered T cell infiltration into tumors followed by tumor growth suppression [43, 44]. Our study involved assessing the anticancer activity of the synthesized Fe_2O_3 -NPs using human cancer cell lines including HeLa and HepG2. In our case, high activity was noted against HepG2 with an IC_{50} of $71 \mu\text{g}/\text{mL}$. Numerous studies have shown metallic NPs including palladium, zinc, gold, and copper to be effective against HeLa cell lines, while biosynthesized selenium NPs to be effective against HepG2, apart from nickel zinc ferrite, zinc oxide, and silver [45–52]. Studies have identified the cytotoxicity of Fe_2O_3 -NPs on HepG2 to be concentration dependent and found $100 \mu\text{g}/\text{mL}$ to cause a 10% reduction in viability [53]. Studies have also constructed and characterized Fe_2O_3 -NPs for intracellular delivery of anthracycline doxorubicin for tumor cell inactivation. This study found treatment with anthracycline doxorubicin Fe_2O_3 -NPs to decrease HeLa cell proliferation in a time- and concentration-dependent manner ($\text{IC}_{50} = 27.5 \pm 12.0 \mu\text{g}/\text{mL}$ after 96 h). These studies highlight the potential of using metallic NPs for efficient targeted chemotherapy.

5. Conclusion

The association of nanotechnology and NPs is slated to ease many of the biological and healthcare issues as physiological activities do occur in the nanoscale. Balancing the negative impact at the cellular level and harnessing the potential of NPs for nanomedicine require personalized research against

each aspect, to identify mode of action and impact of various coatings. The multitarget activity of the NPs has been postulated to be effective against common multidrug-resistant species, and this becomes the need of the hour as overuse of antibiotics across the world continues to fuel emergence of resistant strains. Our study demonstrates the successful generation of Fe_2O_3 -NPs along with its application in the antimicrobial and anticancer avenues. NP-based research has the potential to radicalize the avenue of personalized as well as generic treatment strategies using proteins and small molecules.

Data Availability

The data used to support the findings of this study are included within the article.

Conflicts of Interest

The authors declare no any conflict of interest.

Acknowledgments

The authors extend their appreciation to the Researchers Supporting Project number (RSP-2021/301), King Saud University, Riyadh, Saudi Arabia, for funding this work.

References

- [1] V. Wagner, A. Dullaart, A.-K. Bock, and A. Zweck, “The emerging nanomedicine landscape,” *Nature Biotechnology*, vol. 24, no. 10, pp. 1211–1217, 2006.
- [2] M. J. Mitchell, M. M. Billingsley, R. M. Haley, M. E. Wechsler, N. A. Peppas, and R. Langer, “Engineering precision nanoparticles for drug delivery,” *Nature Reviews Drug Discovery*, vol. 20, no. 2, pp. 101–124, 2021.
- [3] I. Khan, K. Saeed, and I. Khan, “Nanoparticles: properties, applications and toxicities,” *Arabian Journal of Chemistry*, vol. 12, no. 7, pp. 908–931, 2019.
- [4] W.-K. Shin, J. Cho, A. G. Kannan, Y.-S. Lee, and D.-W. Kim, “Cross-linked composite gel polymer electrolyte using mesoporous methacrylate-functionalized SiO_2 nanoparticles for lithium-ion polymer batteries,” *Scientific Reports*, vol. 6, no. 1, pp. 1–10, 2016.
- [5] S. Bamrungsap, Z. Zhao, T. Chen et al., “Nanotechnology in therapeutics: a focus on nanoparticles as a drug delivery system,” *Nanomedicine*, vol. 7, no. 8, pp. 1253–1271, 2012.
- [6] S. Barua, P. P. Banerjee, A. Sadhu et al., “Silver nanoparticles as antibacterial and anticancer materials against human breast, cervical and oral cancer cells,” *Journal of Nanoscience and Nanotechnology*, vol. 17, no. 2, pp. 968–976, 2017.
- [7] B. Du, M. Yu, and J. Zheng, “Transport and interactions of nanoparticles in the kidneys,” *Nature Reviews Materials*, vol. 3, no. 10, pp. 358–374, 2018.
- [8] M.-X. Luo, S. Hua, and Q.-Y. Shang, “Application of nanotechnology in drug delivery systems for respiratory diseases,” *Molecular Medicine Reports*, vol. 23, no. 5, pp. 1–17, 2021.
- [9] S. Hua, M. B. C. de Matos, J. M. Metselaar, and G. Storm, “Current trends and challenges in the clinical translation of nanoparticulate nanomedicines: pathways for translational development

- and commercialization," *Frontiers in Pharmacology*, vol. 9, p. 790, 2018.
- [10] M. Sharland, C. Pulcini, S. Harbarth et al., "Classifying antibiotics in the WHO Essential Medicines List for optimal use—be AWaRe," *The Lancet Infectious Diseases*, vol. 18, no. 1, pp. 18–20, 2018.
- [11] J. F. Mahoney, R. Arnold, and A. Harris, "Penicillin treatment of early syphilis—a preliminary report," *American Journal of Public Health the Nations Health*, vol. 33, no. 12, pp. 1387–1391, 1943.
- [12] R. I. Aminov, "A brief history of the antibiotic era: lessons learned and challenges for the future," *Frontiers in Microbiology*, vol. 1, p. 134, 2010.
- [13] P. Fernandes and E. Martens, "Antibiotics in late clinical development," *Biochemical Pharmacology*, vol. 133, pp. 152–163, 2017.
- [14] Y. N. Slavin, J. Asnis, U. O. Hafeli, and H. Bach, "Metal nanoparticles: understanding the mechanisms behind antibacterial activity," *J Nanobiotechnology*, vol. 15, no. 1, p. 65, 2017.
- [15] C. Bankier, R. K. Matharu, Y. K. Cheong, G. G. Ren, E. Cloutman-Green, and L. Ciric, "Synergistic antibacterial effects of metallic nanoparticle combinations," *Scientific Reports*, vol. 9, no. 1, p. 16074, 2019.
- [16] R. J. Mody, J. R. Prensner, J. Everett, D. W. Parsons, and A. M. Chinnaiyan, "Precision medicine in pediatric oncology: lessons learned and next steps," *Pediatric Blood Cancer*, vol. 64, no. 3, article e26288, 2017.
- [17] M. Buttacavoli, N. N. Albanese, G. Di Cara et al., "Anticancer activity of biogenerated silver nanoparticles: an integrated proteomic investigation," *Oncotarget*, vol. 9, no. 11, pp. 9685–9705, 2018.
- [18] J. Bai Aswathanarayan, R. Rai Vittal, and U. Muddegowda, "Anticancer activity of metal nanoparticles and their peptide conjugates against human colon adenorectal carcinoma cells," *Artif Cells Nanomed Biotechnol*, vol. 46, no. 7, pp. 1444–1451, 2018.
- [19] F. Soetaert, P. Korangath, D. Serantes, S. Fiering, and R. Ivkov, "Cancer therapy with iron oxide nanoparticles: agents of thermal and immune therapies," *Advanced Drug Delivery Reviews*, vol. 163–164, pp. 65–83, 2020.
- [20] A. S. Teja and P.-Y. Koh, "Synthesis, properties, and applications of magnetic iron oxide nanoparticles," *Progress in Crystal Growth Characterization of Materials*, vol. 55, no. 1–2, pp. 22–45, 2009.
- [21] E. Sanchez-Lopez, D. Gomes, G. Esteruelas et al., "Metal-based nanoparticles as antimicrobial agents: an overview," *Nanomaterials*, vol. 10, no. 2, p. 292, 2020.
- [22] M. A. Kalam and A. Alshamsan, "Poly (d, l-lactide-co-glycolide) nanoparticles for sustained release of tacrolimus in rabbit eyes," *Biomedicine and Pharmacotherapy*, vol. 94, pp. 402–411, 2017.
- [23] H. M. Al-Yousef, M. Amina, A. S. Alqahtani et al., "Pollen bee aqueous extract-based synthesis of silver nanoparticles and evaluation of their anti-cancer and anti-bacterial activities," *Processes*, vol. 8, no. 5, p. 524, 2020.
- [24] F. Wang, X. Qin, Y. Meng, Z. Guo, L. Yang, and Y. Ming, "Hydrothermal synthesis and characterization of α -Fe₂O₃ nanoparticles," *Materials Science in Semiconductor Processing*, vol. 16, no. 3, pp. 802–806, 2013.
- [25] P. Mallick and B. Dash, "Chemical Capping Synthesis of Nickel Oxide Nanoparticles and their characterizations Studies," *Nanoscience and Nanotechnology*, vol. 2, no. 5, pp. 134–138, 2012.
- [26] M. Arakha, S. Pal, D. Samantarrai et al., "Antimicrobial activity of iron oxide nanoparticle upon modulation of nanoparticle-bacteria interface," *Scientific Reports*, vol. 5, no. 1, p. 14813, 2015.
- [27] B. S. Inbaraj, T.-Y. Tsai, and B.-H. Chen, "Synthesis, characterization and antibacterial activity of superparamagnetic nanoparticles modified with glycol chitosan," *Science Technology of Advanced Materials*, vol. 13, no. 1, article 015002, 2012.
- [28] S. Hwang, A. Umar, G. Dar, S. Kim, and R. Badran, "Synthesis and characterization of iron oxide nanoparticles for phenyl hydrazine sensor applications," *Sensor Letters*, vol. 12, no. 1, pp. 97–101, 2014.
- [29] P. Sharma, R. Kumar, S. Chauhan, D. Singh, and M. S. Chauhan, "Facile growth and characterization of alpha-Fe₂O₃ nanoparticles for photocatalytic degradation of methyl orange," *Journal of Nanoscience and Nanotechnology*, vol. 14, no. 8, pp. 6153–6157, 2014.
- [30] P. Saharan, G. R. Chaudhary, S. K. Mehta, and A. Umar, "Removal of water contaminants by iron oxide nanomaterials," *Journal of Nanoscience and Nanotechnology*, vol. 14, no. 1, pp. 627–643, 2014.
- [31] P. R. Patil and S. S. Joshi, "Synthesis of α -Fe₂O₃ nanocubes," *Synthesis Reactivity in Inorganic, Metal-Organic, Nano-Metal Chemistry*, vol. 37, no. 6, pp. 425–429, 2007.
- [32] J. R. Costa, N. C. Silva, B. Sarmiento, and M. Pintado, "Potential chitosan-coated alginate nanoparticles for ocular delivery of daptomycin," *European Journal of Clinical Microbiology & Infectious Diseases*, vol. 34, no. 6, pp. 1255–1262, 2015.
- [33] S. Hasany, I. Ahmed, J. Rajan, and A. Rehman, "Systematic review of the preparation techniques of iron oxide magnetic nanoparticles," *Nanoscience and Nanotechnology*, vol. 2, no. 6, pp. 148–158, 2012.
- [34] M. Joya, J. Barón-Jaimez, and J. Barba-Ortega, "Preparation and characterization of Fe₂O₃ nanoparticles," *Journal of Physics: Conference Series*, vol. 466, no. 1, article 012004, 2013.
- [35] S. Saranya, K. Vijayarani, and S. Pavithra, "Green synthesis of iron nanoparticles using aqueous extract of *Musa ornata* flower sheath against pathogenic bacteria," *Indian Journal of Pharmaceutical Sciences*, vol. 79, no. 5, pp. 688–694, 2017.
- [36] F. Batool, M. S. Iqbal, S. U. Khan, J. Khan, B. Ahmed, and M. I. Qadir, "Biologically synthesized iron nanoparticles (FeNPs) from *Phoenix dactylifera* have anti-bacterial activities," *Scientific Reports*, vol. 11, no. 1, p. 22132, 2021.
- [37] S. M. Dadfar, D. Camozzi, M. Darguzyte et al., "Size-isolation of superparamagnetic iron oxide nanoparticles improves MRI, MPI and hyperthermia performance," *Journal of Nanobiotechnology*, vol. 18, no. 1, pp. 1–13, 2020.
- [38] J. Borcherdig, J. Baltrusaitis, H. Chen et al., "Iron oxide nanoparticles induce *Pseudomonas aeruginosa* growth, induce biofilm formation, and inhibit antimicrobial peptide function," *Environmental Science. Nano*, vol. 1, no. 2, pp. 123–132, 2014.
- [39] L.-Y. Zheng and J.-F. Zhu, "Study on antimicrobial activity of chitosan with different molecular weights," *Carbohydrate Polymers*, vol. 54, no. 4, pp. 527–530, 2003.
- [40] S. Chatterjee, A. Bandyopadhyay, and K. Sarkar, "Effect of iron oxide and gold nanoparticles on bacterial growth leading towards biological application," *J Nanobiotechnology*, vol. 9, no. 1, p. 34, 2011.

- [41] Z. H. Kareem, H. K. Shareef, and A. F. Alkaim, "Evaluation of antibacterial activity of Fe^{2+} O^{3-} nanoparticles against *Shigella dysenteriae*," *Journal of Pharmaceutical Sciences Research*, vol. 10, no. 8, pp. 1980–1982, 2018.
- [42] H. S. Devi, M. A. Boda, M. A. Shah, S. Parveen, and A. H. Wani, "Green synthesis of iron oxide nanoparticles using *Platanus orientalis* leaf extract for antifungal activity," *Green Processing and Synthesis*, vol. 8, no. 1, pp. 38–45, 2019.
- [43] P. Korangath, J. D. Barnett, A. Sharma et al., "Nanoparticle interactions with immune cells dominate tumor retention and induce T cell-mediated tumor suppression in models of breast cancer," *Science Advances*, vol. 6, no. 13, p. eaay1601, 2020.
- [44] S. Zanganeh, G. Hutter, R. Spitler et al., "Iron oxide nanoparticles inhibit tumour growth by inducing pro-inflammatory macrophage polarization in tumour tissues," *Nature Nanotechnology*, vol. 11, no. 11, pp. 986–994, 2016.
- [45] M. J. Akhtar, M. Ahamed, S. Kumar, M. M. Khan, J. Ahmad, and S. A. Alrokayan, "Zinc oxide nanoparticles selectively induce apoptosis in human cancer cells through reactive oxygen species," *International Journal of Nanomedicine*, vol. 7, p. 845, 2012.
- [46] M. S. Al-Qubaisi, A. Rasedee, M. H. Flaifel et al., "Induction of apoptosis in cancer cells by NiZn ferrite nanoparticles through mitochondrial cytochrome C release," *International Journal of Nanomedicine*, vol. 8, p. 4115, 2013.
- [47] J. Baharara, T. Ramezani, A. Divsalar, M. Mousavi, and A. Seyedarabi, "Induction of apoptosis by green synthesized gold nanoparticles through activation of caspase-3 and 9 in human cervical cancer cells," *Avicenna Journal of Medical Biotechnology*, vol. 8, no. 2, pp. 75–83, 2016.
- [48] S. Ghosh, R. Nitnavare, A. Dewle et al., "Novel platinum-palladium bimetallic nanoparticles synthesized by *Dioscorea bulbifera*: anticancer and antioxidant activities," *International Journal of Nanomedicine*, vol. 10, pp. 7477–7490, 2015.
- [49] D. Guo, D. Dou, L. Ge, Z. Huang, L. Wang, and N. Gu, "A caffeic acid mediated facile synthesis of silver nanoparticles with powerful anti-cancer activity," *Colloids Surfaces B: Biointerfaces*, vol. 134, pp. 229–234, 2015.
- [50] G. P. Jose, S. Santra, S. K. Mandal, and T. K. Sengupta, "Singlet oxygen mediated DNA degradation by copper nanoparticles: potential towards cytotoxic effect on cancer cells," *Journal of Nanobiotechnology*, vol. 9, no. 1, pp. 1–8, 2011.
- [51] R. Wahab, N. K. Kaushik, A. K. Verma et al., "Fabrication and growth mechanism of ZnO nanostructures and their cytotoxic effect on human brain tumor U87, cervical cancer HeLa, and normal HEK cells," *Journal of Biological Inorganic Chemistry*, vol. 16, no. 3, pp. 431–442, 2011.
- [52] Y. Xia, P. You, F. Xu, J. Liu, and F. Xing, "Novel functionalized selenium nanoparticles for enhanced anti-hepatocarcinoma activity in vitro," *Nanoscale Research Letters*, vol. 10, no. 1, pp. 1–14, 2015.
- [53] L. Sadeghi, F. Tanwir, and V. Y. Babadi, "In vitro toxicity of iron oxide nanoparticle: oxidative damages on Hep G2 cells," *Experimental Toxicologic Pathology*, vol. 67, no. 2, pp. 197–203, 2015.